Accepted Manuscript

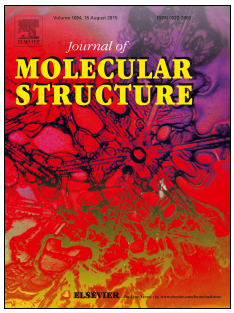

Tuning the molecular/electronic structure of new substituted pyrazoles: Synthesis, biological trials, theoretical approaches and Hammett correlations

Carlos Bustos, Luis Alvarez-Thon, Elies Molins, Ignacio Moreno-Villoslada, Gabriel Vallejos-Contreras, Christian Sánchez, Ximena Zarate, Desmond Mac-Leod Carey, Eduardo Schott

PII: S0022-2860(18)30667-7

DOI: 10.1016/j.molstruc.2018.05.088

Reference: MOLSTR 25261

To appear in: *Journal of Molecular Structure*

Received Date: 29 March 2018

Revised Date: 25 May 2018

Accepted Date: 28 May 2018

Please cite this article as: C. Bustos, L. Alvarez-Thon, E. Molins, I. Moreno-Villoslada, G. Vallejos-Contreras, C. Sánchez, X. Zarate, D. Mac-Leod Carey, E. Schott, Tuning the molecular/electronic structure of new substituted pyrazoles: Synthesis, biological trials, theoretical approaches and Hammett correlations, *Journal of Molecular Structure* (2018), doi: 10.1016/j.molstruc.2018.05.088.

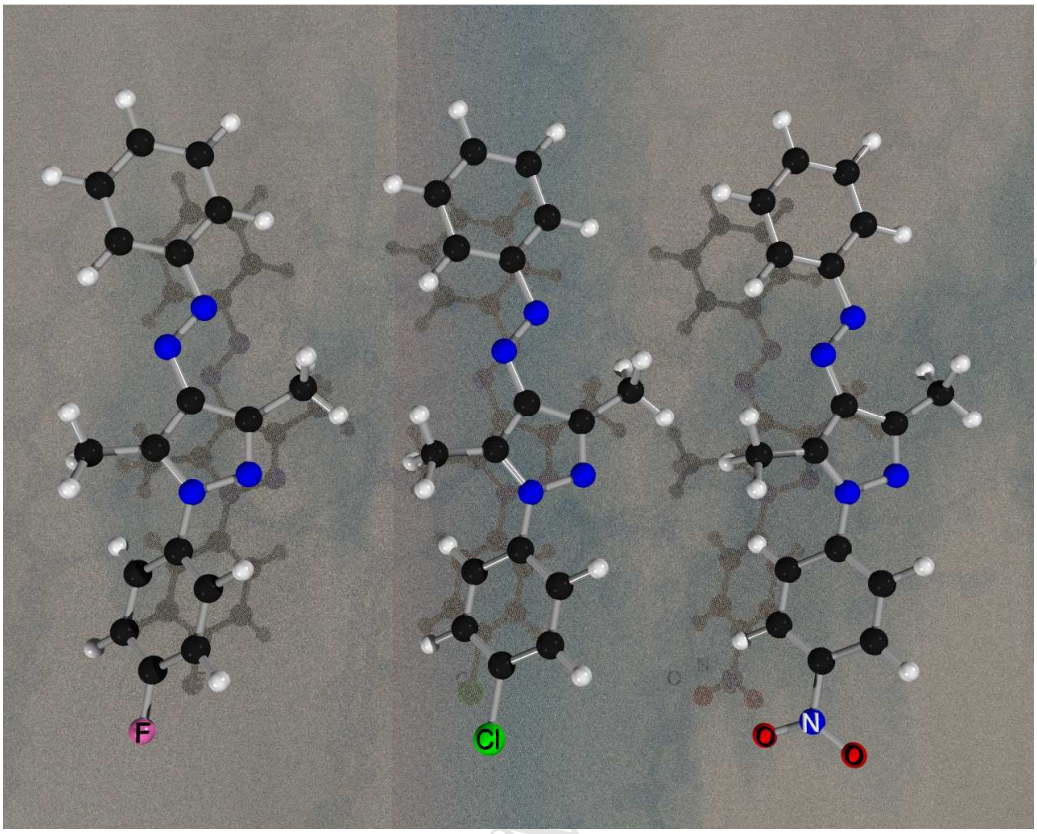

Tuning the molecular/electronic structure of new substituted pyrazoles: synthesis, biological trials, theoretical approaches and Hammett correlations

Carlos Bustos[a*], Luis Alvarez-Thon[b], Elies Molins[c], Ignacio Moreno-Villoslada[a], Gabriel Vallejos-Contreras[a], Christian Sánchez[a], Ximena Zarate[d*], Desmond Mac-Leod Carey[d] and Eduardo Schott[e*]

[a] *Instituto de Ciencias Químicas, Universidad Austral de Chile, Avda. Las Encinas 220, Campus Isla Teja,Casilla 456, Valdivia, Chile.*

[b] *Universidad Central de Chile, Toesca 1783, Santiago de Chile, Chile*

[c] *Institut de Ciència de Materials de Barcelona (ICMAB-CSIC), Campus UAB, 08193 Bellaterra, Spain.*

[d] *Instituto de Ciencias Químicas Aplicadas, Facultad de Ingeniería, Universidad Autónoma de Chile, Av. Pedro de Valdivia 425, Santiago, Chile*

[e] *Departamento de Química Inorgánica, Facultad de Química, Pontificia Universidad Católica de Chile, Vicuña Mackenna 4860, Macul, Santiago.*

Keywords: Pyrazoles; Hammett correlation; Synthesis; DFT; Anticancer activity.

Abstract

The high yield synthesis, characterization and biological trials of a family of compounds containing the pyrazole core (*E*)-3,5-dimethyl-1-(4-**R**-phenyl)-4-(phenyldiazenyl)-1H-pyrazoles (with **R**= 4-CH_3O (**1**), 4-CH_3 (**2**), 4-H (**3**), 4-F (**4**), 4-Cl (**5**), 4-CF_3 (**6**), 4-CN (**7**), 4-NO_2 (**8**), 3-Cl (**9**), 3-NO_2 (**10**), 2-Cl (**11**) and -C_6F_5 (**12**)) are reported. Hammett correlations were found for the experimental and

theoretical computed data, showing the dependence of all the obtained results on the donor or acceptor nature of the R substituent. In this sense, the absorption wavelength does decrease as the electron-withdrawing character of the substituent increases. Furthermore, the wavelength intensity does follow a Hammett correlation with the sigma donor character of the substituents. The compounds were characterized using MP, EA, UV-vis, FT-IR, ^{1}H-NMR, ^{13}C-NMR including bidimensional NMR experiments (HMBC and HMQC). The structures of **4**, **5** and **8** were successfully elucidated by means of X-Ray diffraction. Pyrazole based dyes are known in pharmacological areas. Therefore, biological activity of all these structures were tested against cancer cell lines over a wide library of cell lines (60), including leukemia, colon and brain cancer, showing that the compounds have anticancer activity, which expands the knowledge of this kind of dyes as targets for this critical application. Finally, quantum calculations were carried out in order to give a rational explanation to the observed UV-vis absorption bands and FT-IR signals. As shown, it is possible to tune the molecular/electronic structure of the synthesized dyes by means of changing the -R substituent in the structure.

Introduction

Pyrazole based dyes are fascinating compounds as they have biological activity and several applications in coordination chemistry. These dyes are also pharmacological intermediates and the dyestuff industry uses them[1-7]. It has been reported that many pyrazoles show biological properties such as anti-neoplastic, anti-microbial, anti-inflammatory, anti-diabetic, among others[2–4,8]. Pyrazole derivatives, as biomolecules, have attracted more attention, as they have fascinating pharmacological properties. In the pharmacology industry, the pyrazole ring can be found in a variety of commonly used drugs, that belong to different categories and show diverse therapeutic properties. [9]

Moreover, pyrazoles have much importance in coordination chemistry as the pyrazolates conjugate bases have the ability to generate a bond with metals in different modes and have the ability to generate

strong bridges [1–3]. For instance, complexes containing the pyrazolate ring have been reported as starting material for chemical vapor deposition. For this application they have fascinating luminescent properties[4–7]. The pyrazole ring is possible to be obtained with a variety of previously reported methods[2–4,8]. Those reported procedures are well known and let the synthesis of the pyrazole ring with substituent groups in different positions, which induces changes in their electronic structure, and therefore in their absorption profile[10–12]. Furthermore, pyrazole ring and it pyrazolate form can be considered as polydentate ligands[13–15]. On this subject, the polydentate complex most commonly used in coordination chemistry are polypyrazolylborates[16,17]. The pyrazolium cation, which corresponds to the protonated form of the pyrazole ring, forms part of many salts and, in some cases, their behavior plays an important role as supramolecular guest towards adequate hosts[18–20]. Complexes that have in their structure pyrazolato ligands (one or more) might be synthetized by reacting a pyrazolate anions with a suitable metal salt or trying a mixture pyrazole/metallic salt with a base[21–28].

In terms of acid-base, pyrazoles are amphoteric substances as they can donate or accept protons (H^+). In fact, the free electron pair placed on the N-atom can act as an acceptor in a hydrogen-bond, while the N-H group can act as a donor in a hydrogen-bond. This property (acting as a hydrogen-bond donor) explains the fact that pyrazoles are widely used in supramolecular chemistry. In this context, it has been shown aggregation in solid-state structures of pyrazoles through the N-H group, which is influenced by the character of the substitution in the pyrazole ring[9,28].

Some pyrazole derivatives have interesting applications in the development of new materials, also of new brightening agents. It has been also shown that the pyrazole containing compounds have solvatochromic and electroluminescence properties. Furthermore, pyrazoles can act as semiconductors, liquid crystals, and organic light-emitting diodes. A more complex structure having pyrazole rings in their structure are also of much interest, due to their synthetic utility as synthetic reagents in multicomponent reactions, chiral auxiliaries and guanylating agents. [29]

In order to gain more insight on a pyrazole family of dyes, in the herein article we assess the substituent effect over the molecular, electronic and biological properties of new systems. We reported the study on the synthesis, characterization, anticancer activity and theoretical calculations of a series of twelve (E)-3,5-dimethyl-1-(4-**R**-phenyl)-4-(phenyldiazenyl)-1H-pyrazoles. The -R group has been modified from electron-donor to electron-withdrawing, **R**= 4-CH_3O (**1**), 4-CH_3 (**2**), 4-H (**3**), 4-F (**4**), 4-Cl (**5**), 4-CF_3 (**6**), 4-CN (**7**), 4-NO_2 (**8**), 3-Cl (**9**), 3-NO_2 (**10**), 2-Cl (**11**) and -C_6F_5 (**12**). While changing the -R substituent group, Hammett correlations were found for some of the studied properties (experimental and theoretical data). Those Hammett correlations are dependent on the capacity of the substituent to act as an electron-donor or electron-acceptor in the phenylpyrazole ring. Specifically, the measured main absorption band follows a Hammett correlation (decreasing its value as the electron-withdrawing capacity of the substituent increases). Furthermore, the wavelength intensity does also follow a Hammett correlation with the sigma donor character of the substituents. DFT and TDDFT computations were carried out to get the composition of the frontier molecular orbitals (FMO), to compute the UV-Vis electron promotion and to assign their character. It is shown that is possible to tune the molecular/electronic structure of the synthetized dyes by means of changing the -R substituent in the structure.

Methods and Experimental Procedures

Chemicals. All compounds (aniline, acetic acid, acetylacetone, sodium nitrite, sodium hydroxide, sodium acetate, hydrochloric acid, and substituted arylhydrazines, R-C_6H_4-NH-NH_2 {R=4-CH_3O (**1**), 4-CH_3 (**2**), 4-H (**3**), 4-F (**4**), 4-Cl (**5**), 4-CF_3 (**6**), 4-CN (**7**), 4-NO_2 (**8**), 3-Cl (**9**), 3-NO_2 (**10**), 2-Cl (**11**) and (Perfluorophenyl)hydrazine, NH_2NH-C_6F_5 (**12**)} and solvents (ethanol and $CHCl_3$, $CDCl_3$) were obtained in the common commercial sources (Merck, Fisher and T. J. Baker) and used without purification. The precursor 3-(2-phenylhydrazinylidene)pentane-2,4-dione was synthesized as was previously reported [30,31] and its obtention was checked using FT-IR.

Physical measurements. Melting points were registered on Digital STUARD SMP10 equipment. Elemental analysis was performed on a Fisons EA 1108 micro analyzer. The UV-Visible spectra were recorded in the 1000-250 nm range in a 10 mm quartz cells, using Perkin Elmer Lambda 35 equipment, diluting a concentrated solution ~1.0×10^{-5} mol/L in $CHCl_3$ at ~1.0×10^{-3} mol/L. The IR spectra in solid state were obtained on *ATR Jasco*, PRO450-S, mounted on a *Jasco*, FT/IR-4200 instrument. ^{1}H-NMR, ^{13}C-NMR and bidimensional experiments (HMBC and HMQC) were registered in a 5 mm glass tube at 298 K in $CDCl_3$ solutions using the residual solvent as internal standard, using conventional procedures on a Bruker, AVANCE AM 400 equipment.

Data collection. Single crystals X-Ray diffraction data sets were collected at 293 K, **4** and **5** and 298 K **8** in two different equipment. Compounds **4** and **5** up a max 2θ of *ca.* 52º on a Enraf-Nonius CAD diffractometer and compound **8** up to max 2θ of *ca.* 61º on a Bruker-AXS Smart Apex II diffractometer, using monochromatic MoKα radiation, λ= 0.71069 Å and a 0.3º separation between frames. Data integration was performed using WinGX program in the diffractometer package[32]. Figures 1 exhibit an ORTEP of **4**, **5** and **8**, respectively. Table 1, in the "Description of structures" section, shows selected bonds length and torsion angles. The data collection and structural refinement parameters for each compound are given in Table S1. The structures were solved by direct methods and Fourier's difference, and refined by least squares on F^2 using the SIR-2004 program[33] and the anisotropic displacement parameters for non-H atoms using the SIR-2004 program[33]. All calculations to solve the structures to refine the model proposed and to obtain results were carried out with the computer programs SHELXL97[34]. Crystallographic data (excluding structure factors) for the structures reported in this paper have been deposited with the Cambridge Crystallographic Data Centre as supplementary publication, CCDC No. 295833 for compound (**4**), CCDC No. 295834 for compound (**5**) and CCDC No. 295835 for compound (**8**). Copies of this information may be obtained

free of charge from The Director, CCDC, 12 Union Road, Cambridge CB2 1EZ, UK. Fax: +44 1223 336 033. E-mail: data_request@ccdc.cam.ac.uk. Web page: http://www.ccdc.cam.ac.uk.

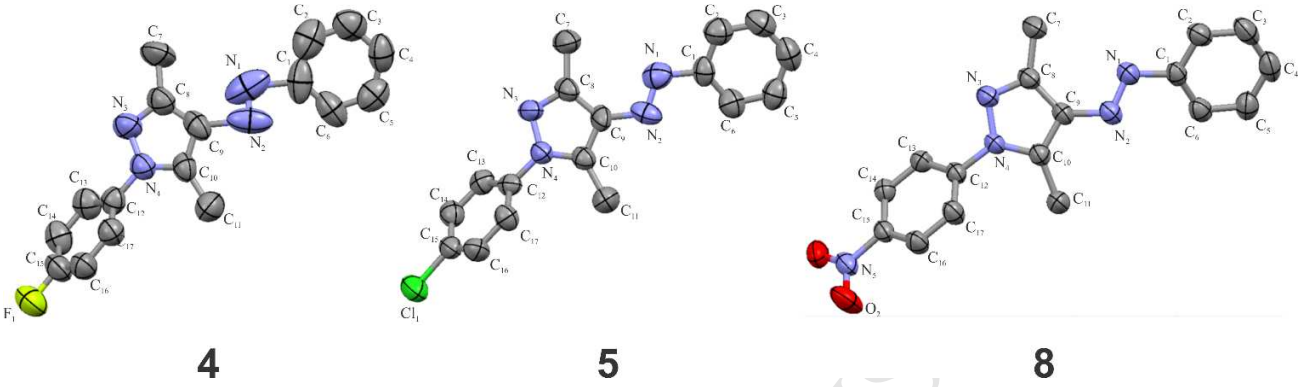

4 5 8

Figure 1. ORTEP view of compounds **4**, **5** and **8** with a probability level of 50%.

Pyrazole Synthesis.

Procedure. In the round-bottomed flask were added 4.9 mmol (1.0 g) of 3-(2-phenylhydrazinylidene)pentane-2,4-dione, 4.9 mmol of any arylhydrazine R-C_6H_4-$NHNH_2$ {R= 4-CH_3O (**1**) 98%, 0.87 g; 4-CH_3 (**2**) 98 %, 0.79 g; 4-H (**3**) 97 %, *d*= 1.099 g/mL, 0.50 mL; 4-F (**4**), 97 % 0.82 g; 4-Cl (**5**) 98 %, 0.89 g; 4-CF_3 (**6**), 96%, 0.90 g; 4-CN (**7**), 97 %, 0.86 g; 4-NO_2 (**8**), 97%, 0.77 g; 3-Cl (**9**), 97 %, 0.90 g; 3-NO_2 (**10**), 98%, 0.95g; 2-Cl (**11**), 97 %, 0.90 g and -C_6F_5 (**12**), 97%, 0.53 g}, 5 mL of glacial acetic acid and 30 mL of ethanol. The reaction mixture was stirred and heated during 36 h near the boiling point. Then, after cool at room temperature, the yellow/orange solid was filtered, washed with water (300 mL) and dried under vacuum for 24 h. All compounds can be recrystallized in ethanol or ethanol/H_2O mixtures of variable composition. Slow evaporation of the ethanol from solutions that contain compounds **4**, **5** and **8** yielded suitable crystals for X-ray diffraction.

(E)-1-(4-methoxyphenyl)-3,5-dimethyl-4-(phenyldiazenyl)-1H-pyrazole **(1).** Yield: 72%. Recrystallized in EtOH/H_2O 9:1, final yield: 58%. MP (ºC): 96-97. EA for $C_{18}H_{18}N_4O$ (Mτ: 306.36 g/mol), Calc.(%) C, 70.57; H, 5.92; N, 18.29; found(%) C, 70.78; H, 6.03; N, 18.33. UV-Visible

spectrum, $CHCl_3$ 1.96×10^{-5} mol/L, λ_{max}, nm(logε): λ_1: 429(3.59), λ_2: 339(4.72). IR spectrum, ν(cm^{-1}): ν(C-H, Ar.): 3051w, 3005w; ν(C-H, Aliph.): 2961w, 2935w, 2921w, 2837w; ν(C=N), ν(C=C) or ν(N=N): 1609w, 1589w, 1552m, 1523s, ν(N-N): 1416s. ^{1}H NMR spectrum (400 MHz, $CDCl_3$) δ ppm: 7.82 (d, *J* = 7.9 Hz, 2H), 7.48 (t, *J* = 7.5 Hz, 2H), 7.39 (t, *J* = 7.5 Hz, 3H), 7.01 (d, *J* = 8.7 Hz, 2H), 3.86 (s, 3H), 2.61 (s, 3H), 2.60 (s, 3H). ^{13}C NMR spectrum (101 MHz in $CDCl_3$) δ ppm: 159.46, 153.75, 143.75, 139.10, 136.04, 132.27, 129.57, 129.03, 126.54, 121.96, 114.48, 55.68, 14.11, 11.35.

(E)-3,5-dimethyl-4-(phenyldiazenyl)-1-p-tolyl-1H-pyrazole (**2**): Crude yield: 92%. Recrystallized in EtOH, final yield 78%. MP (ºC): 84-85. EA for $C_{18}H_{18}N_4$ (Mτ: 290.36 g/mol): Calc.(%): C, 74.46; H, 6.25; N , 19.30; found(%): C, 74.31; H, 6.30; N, 19.40. UV-Visible spectrum, $CHCl_3$ 1.03×10^{-5} mol/L, $\lambda_{max,}$ nm(logε): λ_1: 430(3.81), λ_2: 339(4.94). IR spectrum, ν(cm^{-1}): ν(C-H, Ar.): 3060w, 3034w; ν(C-H, Aliph.): 2965w, 2924w, 2857w; ν(C=N), ν(N=N) or ν(C=C): 1610w, 1587w, 1553m, 1520s, ν(N-N): 1410s. ^{1}H NMR spectrum (400 MHz, $CDCl_3$) δ ppm: 7.83 (d, *J* = 7.8 Hz, 2H), 7.48 (t, *J* = 7.6 Hz, 2H), 7.43 -7.34 (m, 3H), 7.30 (d, *J* = 8.1 Hz, 2H), 2.64 (s, 3H), 2.61 (s, 3H), 2.43 (s, 3H). ^{13}C NMR spectrum (101 MHz, $CDCl_3$) δ ppm: 153.76, 143.82, 139.11, 138.19, 136.76, 136.21, 129.89, 129.59, 129.03, 124.89, 121.97, 21.25, 14.17, 11.43.

(E)-3,5-dimethyl-1-phenyl-4-(phenyldiazenyl)-1H-pyrazole (**3**): Crude yield: 97%. Recrystallized in EtOH, final yield: 81%. MP(ºC): 59-60. EA for $C_{17}H_{16}N_4$ (Mτ: 276.34 g/mol): Calc.(%): C, 73.89; H, 5.84; N, 20.27; found(%):C, 74.02; H, 5.94; N, 20.04. UV-Visible spectrum, $CHCl_3$ 1.00×10^{-5} mol/L, λ_{max}, nm(logε): λ_1: 430(3.84), λ_2: 337(4.99). IR spectrum, ν(cm^{-1}): ν(C-H, Ar.): 3060w, 3035w; ν(C-H, Aliph.): 2962w, 2918w; ν(C=N), ν(N=N) or ν(C=C): 1599m, 1554m, 1509s; ν(N-N): 1411s. ^{1}H NMR spectrum (400 MHz, $CDCl_3$) δ ppm: 7.83 (d, *J* = 7.8 Hz, 2H), 7.56-7.36 (m, 8H), 2.67 (s, 3H), 2.60 (s, 3H). ^{13}C NMR spectrum (101 MHz, *$CDCl_3$*) δ ppm: 153.77, 144.04, 139.29, 139.22, 136.37, 129.70, 129.38, 129.08, 128.21, 125.06, 122.03, 14.21, 11.51.

(E)-1-(4-fluorophenyl)-3,5-dimethyl-4-(phenyldiazenyl)-1H-pyrazole (**4**): Crude yield: 75%.

Recrystallized in EtOH, final yield 66.0%. MP(ºC): 125-126. EA for $C_{17}H_{15}FN_4$ (Mτ: 294,33 g/mol): Calc.(%): C, 69.37; H, 5.14; N, 19.04; found(%): C, 69.36; H, 5.43; N, 19.12. UV-Visible spectrum, $CHCl_3$ 9.85×10^{-6} mol/L, λ_{max}, nm(logε): λ_1: 435(3.98); λ_2: 337 (5.02). IR spectrum, ν(cm^{-1}): ν(C-H, Ar.): 3065w, 3034w; ν(C-H, Aliph.): 2988w, 2967w, 2927w; ν(C=N), ν(N=N) y/o ν(C=C): 1604w, 1557w, 1542w, 1514s; ν(N-N): 1409m. ^{1}H NMR (400 MHz, $CDCl_3$) δ ppm: 7.82 (d, *J* = 7.9 Hz, 2H), 7.47 (t, *J* = 7.1 Hz, 4H), 7.39 (t, *J* = 7.2 Hz, 1H), 7.19 (t, *J* = 8.0 Hz, 2H), 2.62 (s, 3H), 2.58 (s, 3H). ^{13}C NMR (101 MHz, $CDCl_3$) δ ppm: 162.18 (d, *J* = 248.4 Hz), 153.68 (s), 144.13 (s), 139.16 (s), 136.28 (s), 135.38 (d, *J* = 3.0 Hz), 129.77 (s), 129.08 (s), 126.92 (d, *J* = 8.7 Hz), 122.03 (s), 116.32 (d, *J* = 23.0 Hz), 14.13 (s), 11.38 (s).

(E)-1-(4-chlorophenyl)-3,5-dimethyl-4-(phenyldiazenyl)-1H-pyrazole (**5**): Crude yield: 60%. Recrystallized in EtOH, final yield: 43%. MP(ºC): 141-142. EA for $C_{17}H_{15}ClN_4$ (Mτ: 310.78 g/mol), Calc.(%): C, 65.70; H, 4.86; N, 18.03; found(%): C, 65.75; H, 4.89; N, 18.02. UV-Visible spectrum, $CHCl_3$ 1.0×10^{-6} mol/L, λ_{max}, nm(logε): λ_1: 435(3.84); λ_2: 336(4.93). IR spectrum, ν(cm^{-1}): ν(C-H, Ar): 3064w, 3033w; ν(C-H, Aliph.): 2988w, 2963w, 2926w, 2853w; ν(C=N), ν(N=N) y/o ν(C=C):1594w, 1585w, 1556m, 1542w, 1504s; ν(N-N): 1406s. ^{1}H NMR spectrum (400 MHz, $CDCl_3$) δ ppm: 7.82 (d, *J* = 7.5 Hz, 2H), 7.52-7.43 (m, 6H), 7.40 (t, *J* = 7.3 Hz, 1H), 2.66 (s, 3H), 2.59 (s, 3H). ^{13}C NMR spectrum (101 MHz, *$CDCl_3$*) δ ppm: 153.67, 144.34, 139.19, 137.77, 136.49, 133.98, 129.86, 129.57, 129.10, 126.11, 122.06, 14.18, 11.51.

(E)-3,5-dimethyl-4-(phenyldiazenyl)-1-(4-(trifluoromethyl)phenyl)-1H-pyrazole (**6**): crude yield: 90%. Recrystallized in EtOH/H_2O 1:8, final yield: 73.5%. MP (ºC): 109-110. EA for para $C_{18}H_{15}F_3N_4$ (Mτ: 344,33 g/mol): Calc.(%): C, 62.79; H, 4.39; N, 16.27; found(%): C, 62.72; H, 4.45; N, 16.63. UV-Visible spectrum, $CHCl_3$ 9.87×10^{-6} mol/L, λ_{max}, nm(logε): λ_1: 430(3.80), λ_2: 335(4.92). IR spectrum, ν(cm^{-1}): ν(C-H, Ar.): 3083d, 3057d; ν(C-H, Aliph.): 2969w, 2926w; ν(C=N), ν(N=N) y/o ν(C=C): 1613m, 1593w, 1560m, 1523m; ν(N-N): 1410s. ^{1}H NMR (400 MHz, $CDCl_3$) δ ppm: 7.84 (d, *J* = 7.5

Hz, 2H), 7.78 (d, *J* = 8.5 Hz, 2H), 7.67 (d, *J* = 8.4 Hz, 2H), 7.49 (t, *J* = 7.6 Hz, 2H), 7.41 (t, *J* = 7.2 Hz, 1H), 2.72 (s, 3H), 2.61 (s, 3H). ^{13}C NMR spectrum (101 MHz, $CDCl_3$) δ ppm: 153.60, 144.70, 142.11, 139.42, 136.82, 129.99, 129.11, 129.85 (q, *J* = 33.1 Hz), 126.58 (q, *J* = 3.7 Hz), 124.64, 123.92 (q, *J* = 272.2 Hz), 122.10, 14.27, 11.63.

(E)-4-(3,5-dimethyl-4-(phenyldiazenyl)-1H-pyrazol-1-yl)benzonitrile (**7**). Crude yield: 91%, recrystallized in EtOH, final yield: 80.5%. MP(ºC): 197-198. EA for $C_{18}H_{15}N_5$ (Mτ: 301.35 g/mol): Calc.(%): C, 71.74; H, 5.02; N, 23.24; found(%): C, 71.99; H, 4.98; N, 23.04. UV-Visible spectrum, $CHCl_3$ 1.00×10^{-6} mol/L, λ_{max}, nm(logε): λ_1: 437(3.60); λ_2: 335(4.70). IR spectrum, ν(cm^{-1}): ν(C-H, Ar): 3081w, 3057w, 3031w; ν(C-H, Aliph.): 2994w, 2963w, 2925w, 2854w; ν(C≡N): 2221m; ν(C=N), ν(N=N) or ν(C=C): 1601m, 1580w, 1556m, 1541s; ν(N-N): 1404s. ^{1}H NMR spectrum (400 MHz, $CDCl_3$) δ ppm: 7.82 (dd, *J* = 12.0, 8.1 Hz, 4H), 7.70 (d, *J* = 8.1 Hz, 2H), 7.49 (t, *J* = 7.5 Hz, 2H), 7.41 (dd, *J* = 16.6, 9.5 Hz, 1H), 2.75 (s, 3H), 2.59 (s, 3H). ^{13}C NMR spectrum (101 MHz, $CDCl_3$) δ ppm 153.52, 145.10, 142.83, 139.54, 137.12, 133.40, 130.15, 129.13, 124.49, 122.13, 118.27, 111.22, 14.35, 11.80.

(E)-3,5-dimethyl-1-(4-nitrophenyl)-4-(phenyldiazenyl)-1H-pyrazole (**8**): Crude yield: 89%. Recrystallized in EtOH, final yield 72.0%. MP (ºC): 196-197. EA for $C_{17}H_{15}N_5O_2$ (Mτ: 321,33 g/mol): Calc.(%): C, 63.54; H, 4.71; N, 21.79; found(%): C, 63,52 ; H, 4.81; N, 22.03. UV-Visible spectrum, $CHCl_3$ 1.00×10^{-6} mol/L, λ_{max}, nm(logε): λ_1: 431(3.86); λ_2: 334(5.08). IR spectrum, ν(cm^{-1}): ν(C-H, Ar.): 3080w; ν(C-H, Aliph.): 2967w, 2928w, 2844w; ν(C=N), ν(N=N) y/o ν(C=C): 1609w. 1595s, 1561s, 1522s, 1507s; ν(N-N): 1407s. ^{1}H NMR (400 MHz, $CDCl_3$) δ ppm: 8.34 (t, *J* = 10.8 Hz, 2H), 7.78 (dd, *J* = 29.1, 8.2 Hz, 4H), 7.44 (dt, *J* = 14.4, 7.4 Hz, 3H), 2.77 (s, 3H), 2.58 (s, 3H). ^{13}C NMR (101 MHz, $CDCl_3$) δ ppm: 153.51, 146.39, 145.32, 144.38, 139.75, 137.30, 130.23, 129.15, 124.99, 124.17, 122.17, 14.40, 11.92.

(E)-1-(3-chlorophenyl)-3,5-dimethyl-4-(phenyldiazenyl)-1H-pyrazole (**9**). Crude yield: 77%.

Recrystallized in EtOH, final yield: 62%. MP(ºC): 84-85. EA for $C_{17}H_{15}ClN_4$ (Mτ: 310.78 g/mol): Calc.(%): C, 65.70; H, 4.86; N, 18.03; found(%): C, 65.78; H, 4.82; N, 18.34. UV-visible spectrum, $CHCl_3$ 1.0×10^{-6} mol/L, λ_{max}, nm(logε): λ_1: 430(3.28); λ_2: 336(4.49); 257sh. IR spectrum, ν(cm^{-1}): ν(C-H, Ar.): 3079w, 3062w, 3033w; ν(C-H, Aliph.): 2986w, 2955w, 2924w; ν(C=N), ν(N=N) /or ν(C=C): 1596s, 1553s, 1497s; ν(N-N): 1403s. ^{1}H NMR spectrum (400 MHz, $CDCl_3$) δ ppm: 7.83 (d, *J* = 7.9 Hz, 2H), 7.57 (s, 1H), 7.52-7.35 (m, 6H), 2.68 (s, 3H), 2.60 (s, 3H). ^{13}C NMR spectrum (101 MHz, *$CDCl_3$*) δ ppm: 153.60, 144.34, 140.28, 139.30, 136.52, 135.07, 130.26, 129.84, 129.05, 128.16, 125.07, 122.74, 122.04, 14.22, 11.50.

(E)-3,5-dimethyl-1-(3-nitrophenyl)-4-(phenyldiazenyl)-1H-pyrazole (**10**): Crude yield: 85%. Recrystallized in EtOH, final yield: 72%. MP(ºC): 146-147. EA for $C_{17}H_{15}N_5O_2$ (Mτ: 321,33 Calc.(%): C, 63.54; H, 4.71; N, 21.79; found(%): C, 63.51; H, 4.90; N, 22.02. UV-Visible, $CHCl_3$ 1.00×10^{-6} mol/L, λ_{max}, nm(logε): λ_1: 434(3.28); λ_2: 334(4.43). IR spectrum, ν(cm^{-1}): ν(C-H, Ar.): 3109w, 3071w; ν(C-H, Alif.): 2986w, 2971w, 2925w; ν(C=N), ν(N=N) y/o ν(C=C): 1614w, 1559m, 1526s; ν(N-N): 1410m. ^{1}H NMR (400 MHz, $CDCl_3$) δ ppm: 8.44 (s, 1H), 8.26 (d, *J* = 8.2 Hz, 1H), 7.92 (d, *J* = 8.0 Hz, 1H), 7.84 (d, *J* = 7.9 Hz, 2H), 7.70 (t, *J* = 8.1 Hz, 1H), 7.49 (t, *J* = 7.5 Hz, 2H), 7.42 (t, *J* = 7.1 Hz, 1H), 2.76 (s, 3H), 2.60 (s, 3H). ^{13}C NMR (101 MHz, $CDCl_3$) δ ppm: 153.55, 148.79, 145.01, 140.38, 139.47, 136.92, 130.35, 130.13, 130.04, 129.14, 122.41, 122.15, 119.37, 14.30, 11.65.

(E)-1-(2-chlorophenyl)-3,5-dimethyl-4-(phenyldiazenyl)-1H-pyrazole (**11**): Crude yield: 93%. Recrystallized in EtOH, final yield: 72%. MP(ºC): 78-79. EA for $C_{17}H_{15}ClN_4$ (Mτ: 310.78 g/mol): Calc.(%): C, 65.70; H, 4.86; N, 18.03; found(%): C, 65.81; H, 4.90; N, 18.05. UV-Visible spectrum, $CDCl_3$$1.00\times10^{-6}$ mol/L, λ_{max}, nm(logε): λ_1: 428(3.49); λ_2: 333(4.73). IR spectrum, ν(cm^{-1}): ν(C-H, Ar): 3080w, 3066w, 3034w; ν(C-H, Aliph.): 2962dw, 2923w, 2853w; ν(C=N), ν(N=N) or ν(C=C): 1590w, 1580w, 1552m, 1536s, 1510m; ν(N-N): 1416s. ^{1}H NMR spectrum (400 MHz, $CDCl_3$) δ ppm: 7.83 (d, *J* = 8.0 Hz, 2H), 7.62-7.33 (m, 7H), 2.61 (s, 3H), 2.48 (s, 3H). ^{13}C NMR (101 MHz, $CDCl_3$) δ ppm:

153.72, 144.61, 140.70, 136.81, 135.59, 132.52, 130.85, 130.49, 129.87, 129.73, 129.06, 127.90, 122.03, 14.14, 10.72.

(E)-3,5-dimethyl-1-(perfluorophenyl)-4-(phenyldiazenyl)-1H-pyrazole (**12**): Crude yield: 96%. Recrystallized in EtOH, final yield 86%. MP(ºC): 79-80. EA for $C_{17}H_{11}F_5N_4$ (Mτ: 366.29. Calc.(%): C, 55.74; H, 3.03; N, 15.30; found(%): C, 55.65; H, 3.21; N,15.60. UV-Visible spectrum, $CHCl_3$ 1.00×10^{-5} mol/L, λ_{max}, nm(logε): λ_1: 432(3.46); λ_2: 327(4.53). IR spectrum, ν(cm^{-1}): ν(C-H, Ar.): 3076w; ν(C-H, Alif.): 2967w, 2928w; ν(C=N), ν(N=N) y/o ν(C=C): 1562w, 1534s, 1512s; ν(N-N): 1411m. ^{1}H NMR (400 MHz, $CDCl_3$) δ ppm: 7.84 (d, *J* = 7.9 Hz, 2H), 7.49 (t, *J* = 7.5 Hz, 2H), 7.42 (t, *J* = 7.1 Hz, 1H), 2.60 (s, 3H), 2.53 (s, 3H). ^{13}C NMR (101 MHz, $CDCl_3$) δ ppm: 153.46 (s), 146.66 (s), 145.53-145.23 (m), 143.83-143.34 (m), 142.83 (ddd, *J* = 11.8, 7.8, 3.9 Hz), 141.54 (s), 141.21-140.80 (m), 139.57 – 139.09 (m), 137.20-136.57 (m), 136.00 (s), 130.25 (s), 129.12 (s), 122.16 (s), 114.46 (td, *J* = 14.2, 4.2 Hz), 14.14 (s), 10.19 (s).

In vitro anti-tumor assays. The NCI's in vitro anti-tumor screening protocol consists of 60 human tumor cell lines against which compounds **1-8** and **12** were tested with 3-4,5-dimethylthiazol-2-yl-2,5-diphenyl-tetrazolium bromide (MTT) assay (11). Cancer cells were treated with 1 μM of test compounds. Dimethyl sulfoxide (DMSO) was used as a vehicle control and six wells were prepared for each compound. After treatment, the supernatant was carefully aspirated and 150 μl of DMSO was added to each well. The absorbance was measured at 590 nm.

Computational details. All the computations were performed in Gaussian 09 [35], performing ground-state geometry optimization with Becke's three-parameter hybrid exchange functional and the Lee-Yang-Parr nonlocal correlation functional including the long-range interaction correction CAM-B3LYP[36–40]. The basis set 6-31G* was used for C, N, O, Cl, Br, and H atoms[41]. The Hessian for all compounds was also calculated to assure them as local minimum (no imaginary values were found). Time-dependent DFT (TDDFT) calculations were also performed using the same theoretical level. The first 60 singlet excited states were computed. Calculations by the first-principles method were used to

obtain accurate excitation energies and oscillator strengths. The effect of the solvent was included with the polarizable continuum model (PCM) using as solvent ethanol[42] for the optimization and TDDFT calculations. See Figure S1 for all the FMO involved in the transitions.

Results and discussion

Synthesis. The compound 3-(2-phenylhydrazinylidene)pentane-2,4-dione, of formula C_6H_5-NHN=C($COCH_3$)$_2$, reacts with substituted arylhydrazines, R-C_6H_4-NH-NH_2, in 1:1 molar ratio, to give in good yields a series of 1,3,4,5-tetrasubstituted pyrazoles **1-12** (See Scheme 1). These reactions were carried out refluxing the reactants during 36 h in EtOH and glacial HOAc as catalyst. The crude products were purified by recrystallization in EtOH or mixtures of EtOH/H_2O of variable composition, under these conditions single crystals of three members of this series were obtained.

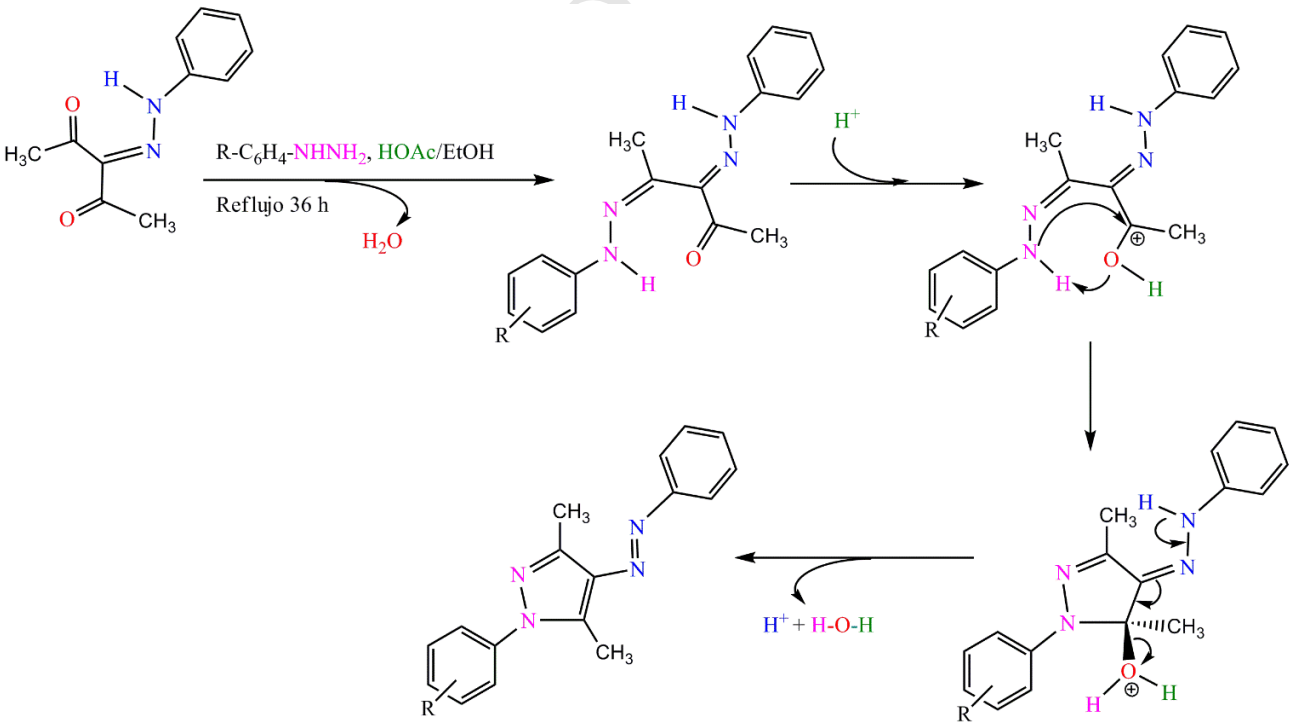

Scheme 1. Proposed reaction mechanism. (**R**=4-CH_3O (**1**), 4-CH_3 (**2**), 4-H (**3**), 4-F (**4**), 4-Cl (**5**), 4-CF_3

(**6**), 4-CN (**7**), 4-NO_2 (**8**), 3-Cl (**9**), 3-NO_2 (**10**), 2-Cl (**11**) and (Perfluorophenyl)hydrazine, NH_2NH-C_6F_5 (**12**)).

In concordance with Scheme 1, it is proposed that the reaction produces the β-dihydrazone as intermediate that, in the course of the heating in acid medium, suffers an addition reaction followed by displacement of one H_2O molecule, yielding the respective pyrazoles[9]. The pure compounds were characterized using analytical techniques (MP and EA), spectroscopic methods (UV-Visible, FT-IR and NMR) and by X-ray diffraction methods the crystalline structures of **4**, **5** and **8** were obtained.

Description of structures. Figure 1 shows the molecular views of compounds **4**, **5** and **8**. In the Supplementary Material, in Table S1 are provided a survey of crystallographic and refinement data for the three compounds. Moreover, Table 1 shows some selected bond distances, angles, torsion angles and the DFT results for the geometry optimizations. The discussion of the DFT data will be further mentioned in the theoretical calculation section.

These structures have been well refined with final R indices with [$I>2\sigma(I)$] of *R1*= 0.0752, w*R2* =0.1202 **4**, *R1*= 0.0751, *wR2*= 0.1302 **5** and *R1*=0.071, *wR2*=0.1565 **8**, see Table S1. Further information concerning the resolution of these structures can be seen in the Supplementary Material. Compounds **4**, **5** and **8** are isostructural and the presence of the pyrazole ring confirms the cyclization reaction proposed in the mechanism of Scheme 1. Furthermore, the azo bridge adopts *E* configuration (see Figure 1). The torsion angle measured between the planes generated by each ring show that these structures are not planar and therefore no electronic communication in the structure might be expected. The measured distances in the three compounds for N_1-N_2 are consistent with the presence of a double bond and the distances N_1-C_1 and N_2-C_9 are consistent with single bonds, see Table 1. Furthermore, the proximity to 120º of the angles C_1-N_1-N_2 indicate that both nitrogen atoms, N_1 and N_2, have a marked sp^2 character. In case of **4**, a certain degree of disorder is observed. Similar previously reported

structures were found in literature and a comparison between the herein reported and the previously reported results[43] are also shown in Table 1. The previous reported structure showed a cyanide group in the azophenyl ring. All other reported compounds show a good correlation between bond distances, angles and the torsion angle involved in the molecules. Finally, there are no conventional intermolecular and intramolecular hydrogen bonds in **4**, **5** and **8** and the whole supramolecular structure is built by weak interactions. However, the nitro group plays a crucial role in the crystal packing of **8** since two NO_2 groups of neighboring molecules are linked *via* a dipole-dipole interaction. This special interaction involving to the nitro-group has been described as type V interaction in the literature[44]. Details on the supramolecular structure of each compound are shown in the SI.

Table 1. Geometrical parameters (in Å) at DFT theoretical level are reported for compounds **1**-**12**. For 4, 5 and 8, the experimental data obtained from the X-Ray structures are labelled with (exp).

Distance	**$-N_1=N_2-$**	**$-C_9-N_2=$**	**$=N_1-C_1-$**	**$-N_3-N_4-$**	**$-N_4-C_{12}-$**	**$-C_1-N_2=N_1-$**	**$-N_2=N_1-C_9$**
1	1.252	1.422	1.386	1.365	1.421	114.8	115.8
2	1.252	1.422	1.386	1.366	1.420	114.8	115.8
3	1.252	1.422	1.386	1.366	1.420	114.8	1.4
4	1.252	1.422	1.387	1.366	1.419	114.8	115.7
4_{EXP}	1.077	1.667	1.675	1.386	1.426	91.9	90.4
5	1.252	1.422	1.387	1.366	1.418	114.9	115.7
5_{EXP}	1.222	1.470	1.440	1.379	1.426	111.8	112.6
6	1.251	1.421	1.388	1.367	1.415	114.9	115.6
7	1.251	1.421	1.388	1.368	1.414	114.9	115.6
8	1.251	1.421	1.389	1.368	1.412	115.0	115.5
8_{EXP}	1.250	1.432	1.404	1.381	1.423	113.0	114.8
9	1.252	1.422	1.387	1.366	1.417	114.9	115.7
10	1.251	1.421	1.388	1.367	1.414	114.9	115.5
11	1.252	1.422	1.387	1.366	1.418	114.8	115.7
12	1.251	1.422	1.389	1.368	1.405	114.9	115.5
[43]*	1.188	1.440	1.567	1.372	1.408	102.4	106.2

*(E)-4-(3,5-dimethyl-1-(perfluorophenyl)-1H-pyrazol-4-yl)diazenyl)benzonitrile

Spectroscopic studies. The UV-vis spectra of compounds **1-12** exhibit two main absorption bands. Both bands character was assigned using TDDFT calculation (*vide infra*). The most intense, λ_1, is

located in the range 327-339 nm (logε=4.43-5.08) and is attributed to the $\pi^* \leftarrow \pi$ transition centered in the group -C-N=N-C-, which is conjugated with the pyrazolyl and phenyl rings in each compound. On the other hand, the absorption band placed at lower energy, λ_2, has lower intensity and it is centered in the range 428-437 nm. In all compounds this absorption appears as a shoulder besides λ_1 or has some contribution of λ_1, which increases the absorption coefficient of λ_2 at values within the range logε=3.28-3.98, see Figure 2 and the SI. According with the above observation, it is proposed that λ_2 is a $\pi^* \leftarrow n$ transition that emerges from the azo group, -N=N-, present in each molecule. The UV-vis spectra of each compound may be found in Figure 2. The absorption maxima are summarized in Table 2. Further discussion might be found in the theoretical calculation section.

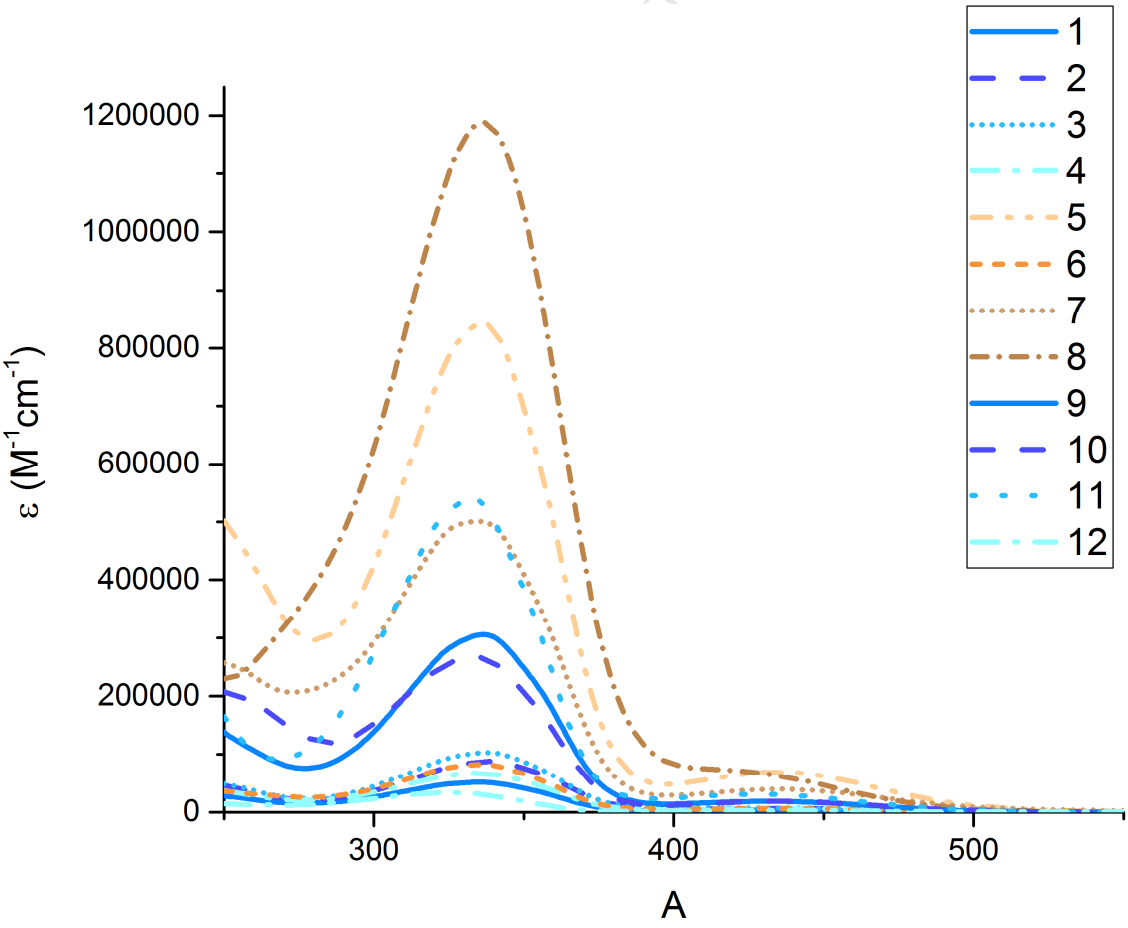

Figure 2. Experimental UV–vis absorption spectrum in $CHCl_3$.

Table 2. Hammett constant value (σ), UV-Vis (exp) and TDDFT calculations (Th) for all the studied compounds, oscillator strength (*f*), involved molecular orbitals and contribution (%).

Comp.	σ_t	λ_{exp}	logε	eV	λ_{Th}	f	Transition			%
1	-0.27	429	3.59	2.97	418	0.0001	HOMO	→	LUMO	85
							HOMO-1	→	LUMO	15
		339	4.72	3.81	325	1.1464	HOMO-1	→	LUMO	70
							HOMO-4	→	LUMO	13
2	-0.17	430	3.81	2.96	418	0.0000	HOMO	→	LUMO	96
		339	4.94	3.82	324	1.1490	HOMO-3	→	LUMO	80
							HOMO	→	LUMO+3	12
3	0	430	3.84	2.96	419	0.0000	HOMO	→	LUMO	100
		337	4.99	3.84	323	1.1253	HOMO-1	→	LUMO	97
4	0.06	435	3.98	2.96	419	0.0000	HOMO	→	LUMO	100
		337	4.89	3.85	322	1.1153	HOMO-1	→	LUMO	97
5	0.23	435	3.84	2.96	419	0.0000	HOMO	→	LUMO	98
		336	4.93	3.84	323	1.1891	HOMO-1	→	LUMO	91
6	0.54	430	3.8	2.95	420	0.0001	HOMO	→	LUMO	100
		335	4.92	3.85	322	1.1958	HOMO-1	→	LUMO	94
7	0.66	437	3.6	2.95	420	0.0001	HOMO	→	LUMO	96
		335	4.7	3.83	323	1.3382	HOMO-1	→	LUMO	87
							HOMO-1	→	LUMO+1	13
8	0.78	431	3.86	2.94	421	0.0002	HOMO	→	LUMO+1	52
							HOMO	→	LUMO	42
		334	5.08	3.77	329	1.4864	HOMO-1	→	LUMO+1	87
							HOMO-1	→	LUMO	10
9	0.37	430	3.28	2.96	419	0.0003	HOMO	→	LUMO	100
		336	4.49	3.85	322	1.1611	HOMO-1	→	LUMO	98
10	0.71	434	3.28	2.95	420	0.0000	HOMO-1	→	LUMO	96
		334	4.43	3.86	321	1.1763	HOMO-2	→	LUMO	98
11		428	3.49	2.97	417	0.0002	HOMO	→	LUMO	100
		333	4.73	3.91	317	1.0561	HOMO-1	→	LUMO	96
12		432	3.46	2.96	418	0.0000	HOMO	→	LUMO	100
		327	4.53	3.95	314	1.0800	HOMO-1	→	LUMO	97

The main characteristics of the IR spectra of **1-12** show the weak stretching modes ν(C-H), attributed to the aromatic and aliphatic groups over and under 3000 cm^{-1}, respectively. Besides, all compounds display a set of absorptions of variable intensity in the range 1614-1497 cm^{-1}, assigned to the stretching modes ν(C=N), ν(N=N) or ν(C=C). The absorptions located in the range 1416-1403 cm^{-1} have been

assigned to the single ν(N-N) of the pyrazole ring and compound **7** displays the respective stretching mode ν(C≡N) at 2221 cm^{-1}. All the set of IR spectra can be found in the SI.

The ^{1}H-NMR and ^{13}C-NMR spectra of compounds **1-12** were labeled using the numeration shown according to Figure 3, the full summary of the observed signals for each compound and each atom is shown in the SI. The ^{1}H-NMR spectra display the resonances in the range 8.34-7.01 ppm attributed to the aromatic protons. All compounds display two singlets in the ranges 2.77-2.48 ppm and 2.61-2.58 ppm that reveal the presence of the protons H_1 and H_5 assigned to CH_3 groups linked to the pyrazole ring. Besides, compounds **1** and **2** show the typical resonances of the substituent -R, 4-OCH_3 and 4-CH_3 at 3.86 ppm and 2.43 ppm, respectively. Finally, the relative area of these resonances shows a good agreement with the total number of expected protons for each molecule. On the other hand, the total number of carbon resonances observed in the ^{13}C-NMR spectra of **1-12** are consistent with the expected number for each molecule and, the most general features are associated with the pyrazole ring and with the -R groups of the molecules. In fact, we have found that C_1, C_2, C_3, C_4 and C_5 are located in ranges of chemical shift almost invariable around 14.11-14.40 ppm, 143.75-146.66 ppm, 135.59-137.30 ppm, 139.10-141.54 ppm y 10.19-11.92 ppm, respectively. Also, the substituent -R of **1**, 4-OCH_3, **2**, 4-CH_3 and **7**, 4-C≡N, are placed at 55.68 ppm, 21.25 ppm and 111.22 ppm, respectively.

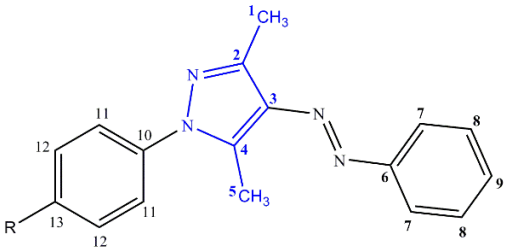

R= 4-CH_3O (**1**), 4-CH_3 (**2**) 4-H (**3**), 4-Cl (**6**), 4-CN (**7**), 4-F (**8**), 4-CF_3 (**9**), 4-NO_2 (**10**)

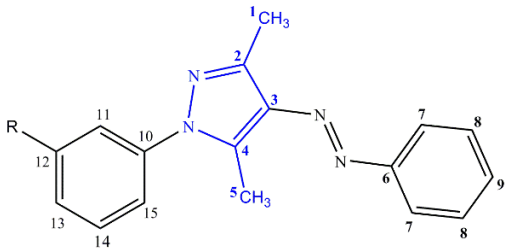

R= 3-Cl (**5**), 3-NO_2 (**11**)

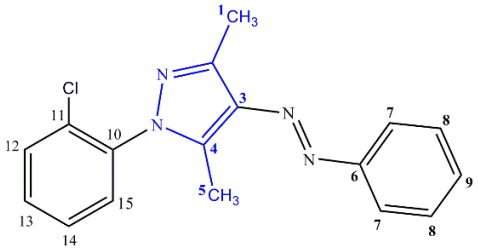

2-Cl (**4**)

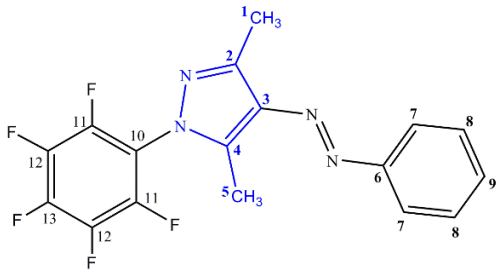

C_6F_5 (**12**)

Figure 3. Used label of hydrogen and carbon atoms for the assignments of the ^{1}H-NMR and ^{13}C-NMR signals of compounds **1**-**12**.

C-F coupling was observed in the carbon resonances of compounds **4**, **6** and **12**. In fact, in case of the 4-F-C_6H_4- group for **4** the four expected resonance signals for carbons C_{13}, C_{12}, C_{11} and C_{10}, appear as doublets in 162.18 ppm ($J_{13\text{-}F}$=248.4 Hz), 116.32 ppm ($J_{12\text{-}F}$=23.0 Hz), 126.92 ppm ($J_{11\text{-}F}$=8.7 Hz) and 135.38 ppm ($J_{10\text{-}F}$=3.0 Hz), respectively. The 4-CF_3-C_6H_4- group of **6** exhibits three quartet attributed to CF_3-, C_{13} and C_{12} in 123.92 ppm ($J_{CF3\text{-}F}$=272.2 Hz), 129.85 ppm ($J_{13\text{-}F}$=33.1 Hz) and 126.58 ppm ($J_{12\text{-}F}$=3.7 Hz), respectively. In this case the signal of C_{10} remain as a singlet. Finally, the C_6F_5- ring of **12** displays a multiplet for C_{10} at 114.33 ppm and, the resonances of the carbons C_{11}, C_{12} and C_{13} emerge as a pair of symmetrical multiplets at 137.97 ppm (J=258.7 Hz), 143.97 ppm (J=255.7 Hz) and 142.17 ppm (J=258.4 Hz), respectively. The $J_{C\text{-}F}$ values observed between each pair of multiplets are in concordance with the geminal C-F coupling; while each multiplet is produced by the C-F coupling at two or more bonds. Figure 4 shows an approximated design of the chemical shift of the signals observed for the C_6F_5- group of **12**.

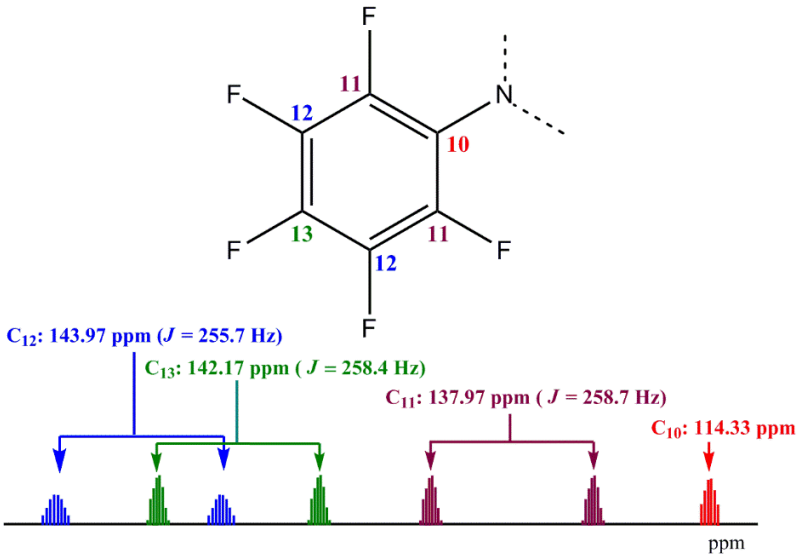

Figure 4. Resonances of carbons C_{10}, C_{11}, C_{12} and C_{13} with C-F coupling displayed by the C_6F_5- group of **12**.

Additional structural information of systems **1**-**12** has been obtained from the bidimensional NMR experiments (HMQC and HBMC). All the HMBC spectra can be found in the SI. In fact, all HMQC and HMBC spectra show the same interaction pattern for the methyl protons with their neighbor carbons located on the pyrazole rings. This pattern is in agreement with the complementary information obtained from the HMQC spectra. To illustrate the common patterns observed in the bidimensional spectra, Figures 5 shows the HMQC spectrum for **12**, where it is possible to observe the main C-H interactions observed in this studied compound.

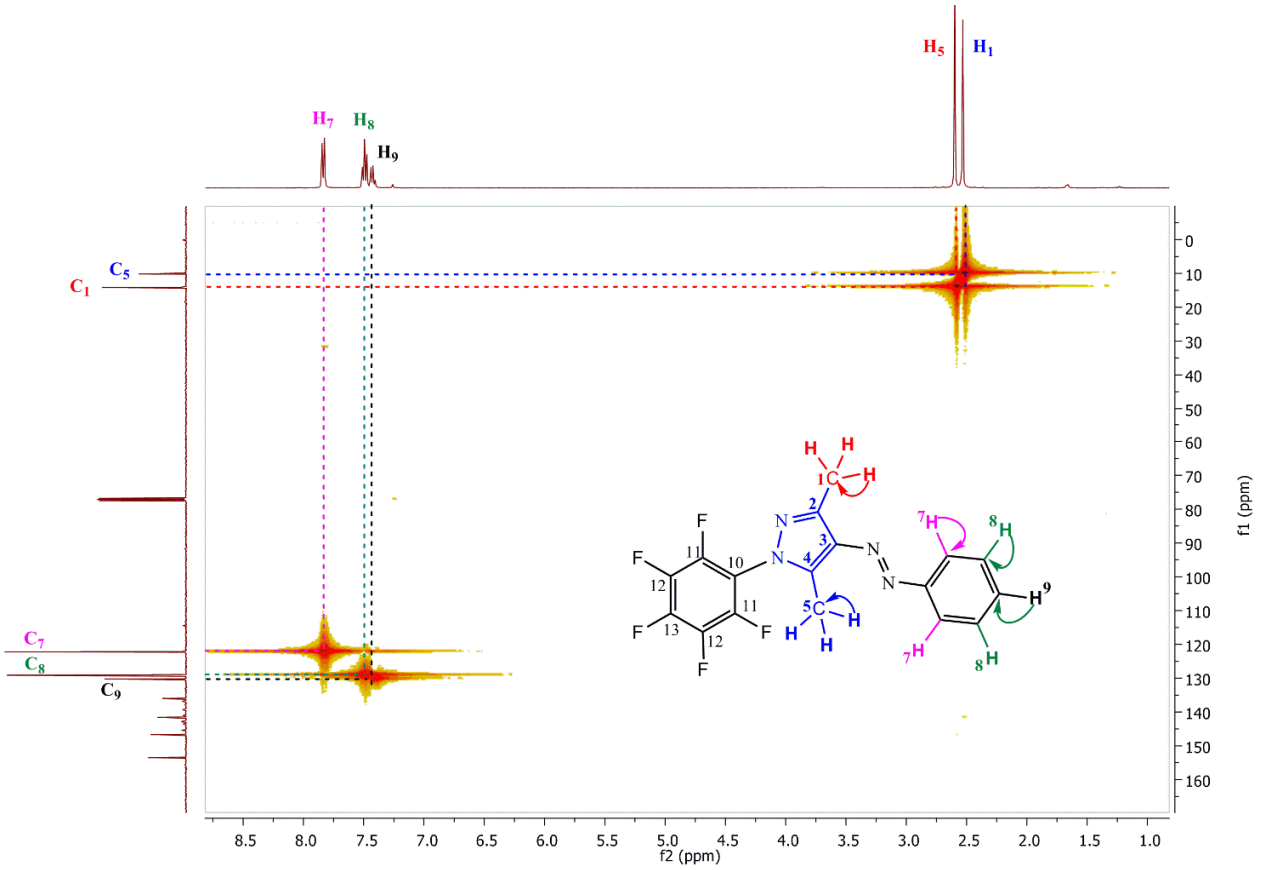

Figure 5. HMQC spectrum of compound **12**.

In vitro anti-tumor assays. Primary in vitro one dose anticancer assay was performed over the full NCI 60 cell panel which include 6 leukemia, 8 melanoma, 9 non-small lung cancer, 7 colon cancer, 6 brain cancer, 8 breast cancer, 6 ovarian cancer, 8 kidney cancer and 2 prostate cancer cell lines. All the experiments were performed in accordance with the protocol of the NCI, USA. One-dose data of all the compounds are reported as a mean graph of the percent growth of treated cells, see Figure 6, 7 and SI. The value obtained for the One-dose assay is referred as growth relative to the control (no-drug), and relative to the time zero number of cells. This allows detection of growth inhibition (values between 0 and 100) and lethality (negative values). For example, a value of 100 means no growth inhibition. A value of 20 would mean 80% growth inhibition. A value of 0 means no net growth during the experiment time. Finally, a value of -50 would mean 50% lethality. A value of -100 means all cells are

dead. The one-dose data of all the compounds is given in the SI.

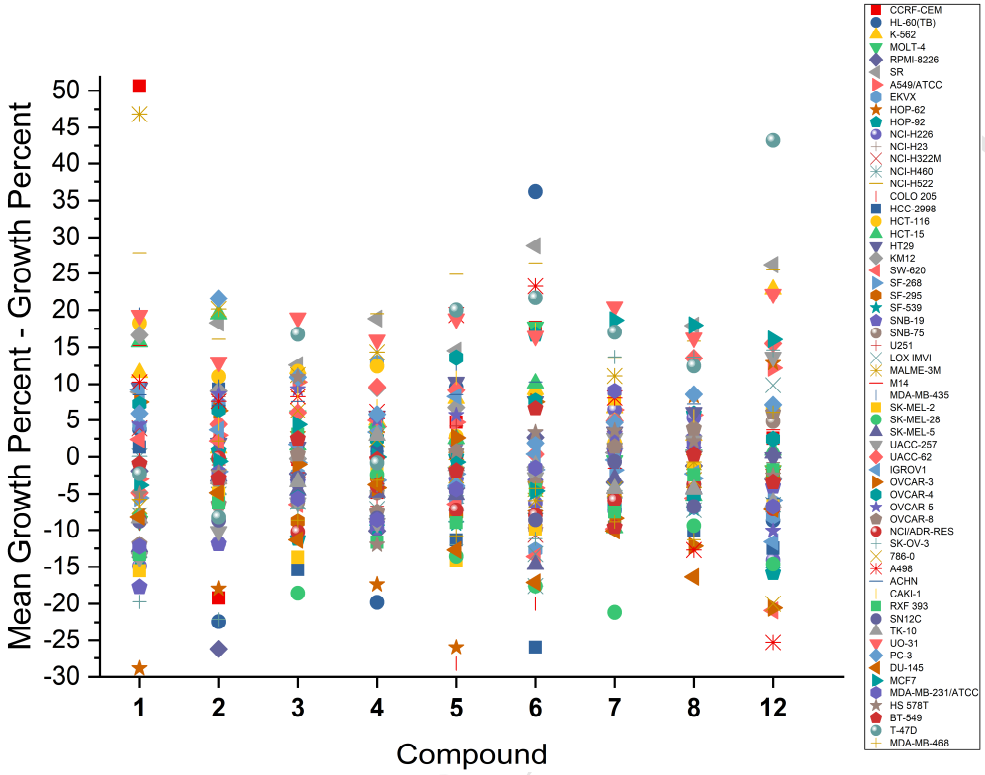

Figure 6. Percentage of cell growth of NCI 60 cancer cell lines displayed by the compounds **1**-**8** and **12**.

As can be observed in Figure 6, all compounds show certain degree of growth inhibition against different cell lines. Furthermore, all compounds also show certain degree of lethality against different cell lines. In this sense, there is no correlation between the activity and the substituent. It is important to notice that highly selective growth inhibition activity was observed against NCI-H522 (lung cancer cell line), UO-31 (kidney cancer cell line) and SR (leukemia cell line) compared to the remaining cell lines, which suggested a certain degree of tumor-tissue-type (disease-oriented) selectivity. Previous reports have shown that the mentioned cell lines (against which the studied compounds were active) commonly

have an over-expression of growth factor kinases (EGFR, HER2/Neu, PDGFR, VEGFR, in between others).[45] On the other hand in terms of lethality, it is observed a clear activity against SK-MEL-28, SK-MEL-28, NCI-H460, DU-145, SN12C, SF-295, SF539 and LOX IMVI. Although, in each of these mentioned cell lines, every compound shows activity, it is only modest. Furthermore, there is no connection of any metabolism in those cell lines, which might be a target of activity of the studied compounds.

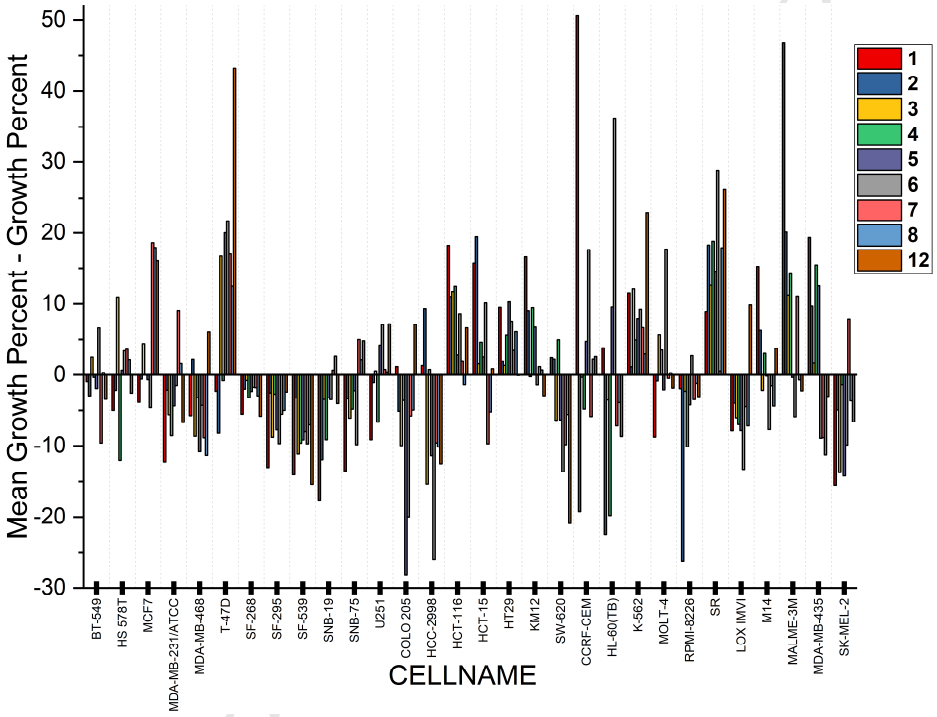

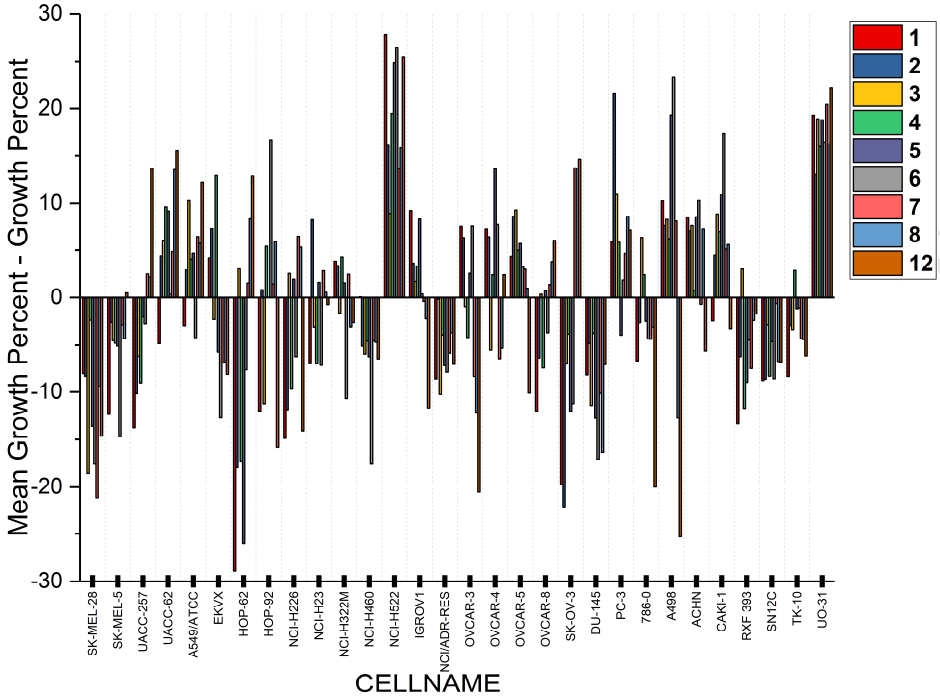

Figure 7. Percentage of cell growth of NCI 60 cancer cell lines displayed by the compounds **1**-**8** and **12** for each cell line.

Theoretical Calculations. To get further understanding of compounds **1**-**12**, theoretical calculations were performed. It is observed that the geometrical parameters of the optimized molecular structures, see Table 1, are in good agreement with the herein X-Ray reported values. Moreover, the bond lengths and angles of the azo group and pyrazole ring are mostly unaffected by the modification of the -R substituent. However, the distances between the phenyl substituted rings and the pyrazole ring get shorter as the substituent over the phenyl ring turns more electron-attracting. This fact is observed when the same substitution positions are compared.

The vibrational frequencies of the optimized structure of each compound were calculated to probe that the obtained structure correspond to an energy minimum. Only positive values were obtained and a good agreement was observed among the experimental and theoretical FT-IR spectra. The superposition of the experimental and theoretical spectra can be found in the SI in figures S2-S13.

Furthermore, in the FT-IR is observed that the vibrations positioned between 1595-1619 cm^{-1} of the experimental FT-IR are assigned to the bonds -C=N- and -N=N- of the chromophores.

To carry out a description of the UV-Vis absorption spectra of **1**-**12**, TDDFT simulations were done. All the involved MOs of the calculated transitions are depicted in the SI (Figure S1). The calculated transition energies show a good agreement with the experimental results. In every case the first calculated transitions located between 421 and 417 nm goes from the HOMO, which is an orbital delocalized over the complete structure, towards the LUMO, which is an orbital located mainly over one side of the molecule. Specifically, in most of the cases, the LUMO is localized over the azo region of the molecule, however in case of the two nitro substituted compounds (**8** and **10**), the LUMO is localized over the phenyl ring that is connected to the pyrazole. The second and most intense calculated transition located in the 329-314nm range, goes from the HOMO-1, which is an orbital located over the azo group, towards the LUMO.

On the other hand, the reactivity indexes are reported in Table 3 (electronic chemical potential (μ), chemical hardness (η), and electrophilicity (ω))[46–48]. η represents the resistance of a reagent to modify its electronic structure[46]. It can be related, such as electronegativity, to the chemical reactivity and stability of a system. In this family of compounds, the biggest value for η is observed for **12**, which has the perfluorinated substituent (being the most electron-attracting substituent). While the smallest value is observed for **1** which has the most electron-donor substituent. μ is related to the direction of the electronic flux during a chemical interaction[46]. This index behaves opposite than the tendency shown by η. In this sense the highest value is shown by **1**, which has the most electron donor substituent. On the other hand, the smallest value is observed for **8**, **10** and **12**, which are the three most electron-attracting substituent. Electrophilicity index, ω, can be defined as the stabilization in energy that an electron acceptor undergoes, when is surrounded by an electron bath at constant electronic chemical potential. The observed values of ω give information whereas in between two molecules, one

behaves as an electrophile (or nucleophile), indicated by a higher (or lower) ω value[47,48]. In this case the highest value of ω was found for compound **10**, which has one of the most electron-attracting substituent. The smallest value is shown by **1**. In this sense, low values of ω indicate an antioxidant behavior, thus the antioxidant potential of these compounds increase as the donor capability of the **R** substituent increases. Therefore, the best antioxidant would be **1**.

Table 3. HOMO and LUMO orbital energies, HOMO-LUMO gap (GAP) and Reactivity indexes, electronic chemical potential (μ), chemical hardness (η) and electrophilicity (ω), all in eV

Comp.	$\sigma_{Hammett}$	HOMO	LUMO	GAP	μ	η	ω
1	-0.27	-7.31	-1.01	6.30	-4.16	3.15	2.75
2	-0.17	-7.41	-1.03	6.38	-4.22	3.19	2.79
3	0	-7.47	-1.05	6.42	-4.26	3.21	2.82
4	0.06	-7.50	-1.07	6.43	-4.28	3.22	2.85
5	0.23	-7.51	-1.09	6.42	-4.30	3.21	2.88
6	0.54	-7.59	-1.15	6.44	-4.37	3.22	2.96
7	0.66	-7.62	-1.23	6.39	-4.42	3.20	3.06
8	0.78	-7.71	-1.25	6.46	-4.48	3.23	3.11
9	0.37	-7.54	-1.10	6.45	-4.32	3.22	2.90
10	0.71	-7.64	-1.24	6.39	-4.44	3.20	3.08
11	-	-7.57	-1.01	6.56	-4.29	3.28	2.81
12	-	-7.73	-1.14	6.59	-4.44	3.30	2.99

Hammett Correlations. To have a clearer description observed for the overall trends due to the modification of the substituent -**R** on the UV-vis absorption wavelengths, geometrical parameters, E_{HOMO}, E_{LUMO}, HL GAP and reactivity indexes, taking into account the substituent electron donor/accepting strength, Hammett constants can be considered a numerical measure of this strength[49]. Contrasts between the two sets of compounds (electron-withdrawing and electron-donor) confirmed a correlation between Hammett parameters and the E_{HOMO} and E_{LUMO} relative to R=H (compound **3**). In case of the geometrical parameters, all measured distances show a Hammett correlation, see SI. As it can be observed, the variation in the calculated geometrical parameters, bond

distances and angles, is small (the variation is observed in the fourth decimal place), however this result shows that the geometrical parameters are only influenced to some extent due to the electron donor/acceptor character of the substituent over the phenyl ring in the pyrazole ring. This is shown by the slope near to zero in each case. The small variations measured for the interatomic distances situated several bonds away from the **-R** group, can be related to the fact that there is small electronic delocalization in the whole molecule.

In case of the energy of the system, as shown in Figure 8 the E_{HOMO} and E_{LUMO}, as the electron-acceptor character of the **-R** group increases, the value of the HL GAP decreases, which is verified by the confluent slopes of the trend lines.

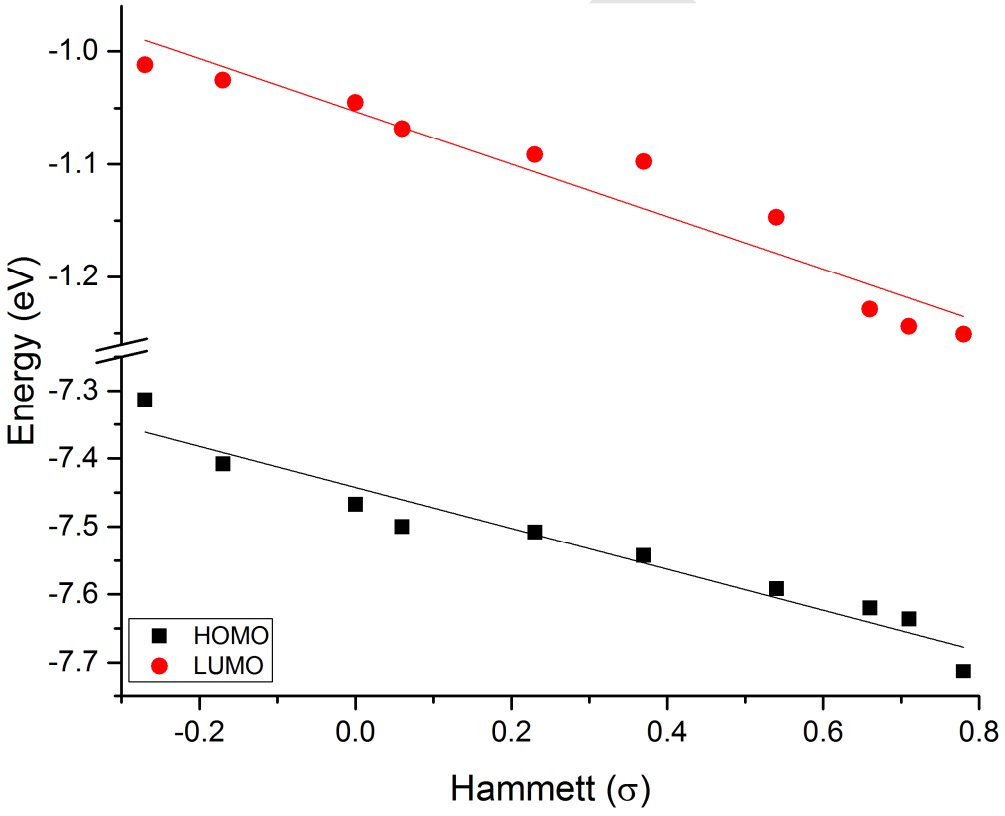

Figure 8. Hammett correlation plot of HOMO (R^2=0.94) and LUMO (R^2=0.93) energies for compounds **1-12**.

In case of the measured UV-vis spectra and TDDFT vertical transitions, a Hammett correlation was

shown in case of the lower wavelength excitation, which has the highest extinction coefficient. It was shown that, as the electron-withdrawing character of the -**R** substituent increase, the absorption wavelength decreases, see Figure 9a. Interestingly, the molar extinction coefficient also follows a Hammett correlation with the sigma donation character of the -**R** substituent. As shown in Figure 9b, as the sigma donation character of the -R substituent decreases, the molar extinction coefficient increases. On the other hand, for the -R substituents with electron-withdrawing sigma donation, the molar extinction coefficient does not follow any trend. finally, the second observed transition involves lower energy MOs and no Hammett correlation was observed.

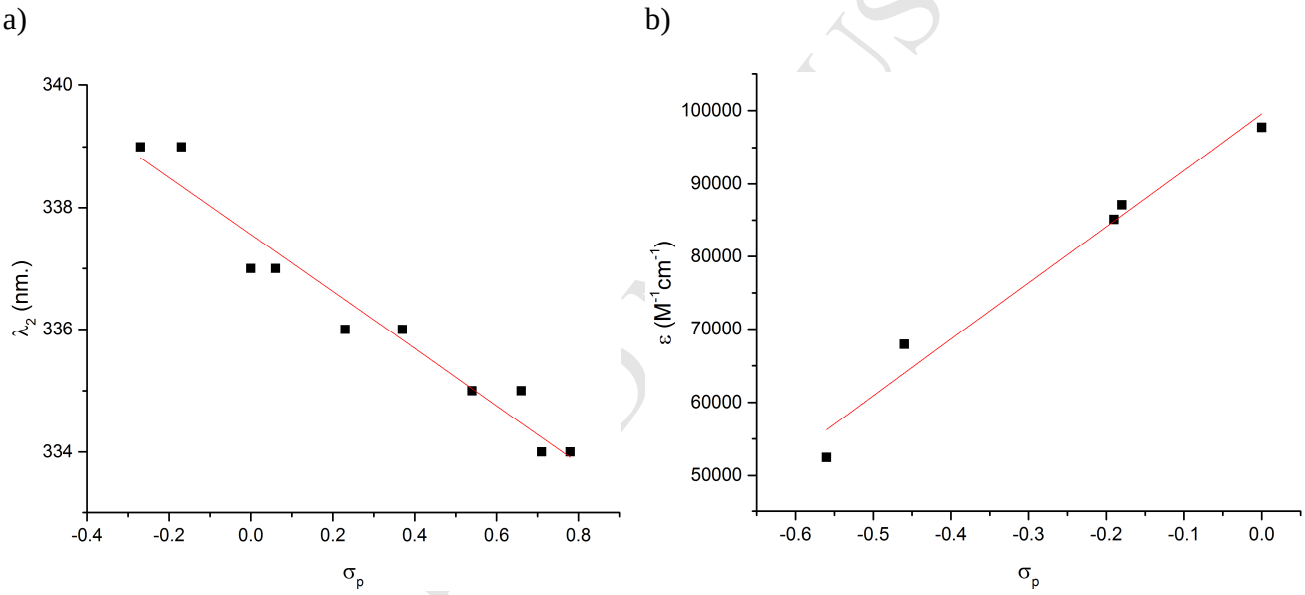

Figure 9. a) Hammett correlation plot of λ_2 absorption wavelength (R^2=0.95). **b)** Hammett correlation plot of ε (R^2=0.97).

In terms of the reactivity indexes, μ and ω show a Hammett correlation with similar trends, as observed before. This shows that the general reactivity of this type of compounds can be tuned, by means of changing the peripheral substituent. See the SI for all the mentioned trends. As shown by the Hammett correlation results, as the electron donor/acceptor character of the substituent changes, the molecular/electronic structure of the studied dyes changes, showing a linear tendency as the substituent

is modified. This allows to tune the measured properties in this family of dyes, by means of changing the -**R** peripheral substituent.

Conclusions

The synthesis of a new family of 12 non-previously reported pyrazoles dyes of the type 3,5-dimethyl-1-(R-phenyl)-4-[(E)-2-phenyldiazen-1-yl]-1H-pyrazole is reported, with high yields. The substituent over the phenyl ring was modified from electron-withdrawing to electron-donor. The nature and type of the substituent induced changes in the geometrical parameters and significant changes over the electronic structure and the prominent reactivity that the compounds might show. These observed effects were studied by means of Hammett correlations. Those results allowed us to propose the tuning in the properties depending on the donor/acceptor character of the -**R** substituent, due to the observed linear tendency as the substituent is modified.

The crystal and molecular structure of three compounds (**4**, **5** and **8**) were determined by single crystal X-ray diffraction. In case of **4**, disorder for the nitrogen atoms was observed in the fragment -C-N=N-C-. This disorder is related to the vibrational coupled mode of this group. The molecule shows a deviation from planarity in the angle generated by the plane of each ring that constitutes the molecule, this fact might be a result of the lack of electronic delocalization. Variable degree of growth inhibition against different cell lines was observed for every compound. Also, all compounds also show certain degree of lethality against different cell lines.

DFT calculations were performed over the studied compounds, and a good correlation between the experimental and theoretical geometrical parameters was observed. Furthermore, no big variations were observed between the studied compounds, which is related to the robustness of the system. Also, the IR and the frequency calculations show a good correlation. Furthermore, TDDFT calculations were performed to obtain the vertical transitions involved in the UV-Vis absorption spectra, showing that the first calculated excitations have involved MOs that are described as $\pi^* \leftarrow \pi$ and the second calculated

transition has a $\pi^* \leftarrow n$ character in all the studied compounds. The antioxidant potential of the herein studied molecules increases as the -**R** substituent increase its donor character. Finally, Hammett correlations, which led assess the tendencies of the influence of the substituents over the phenyl ring and the whole molecule, were found in most of the measured experimental and theoretical properties.

Acknowledgment. Fondecyt 1171118, 1161416 and 11180565. Ministerio de Economía y competitividad of Spain grants SEV 2015-496 and ENE 2015-63969.

References

1. Monica G La, Ardizzoia GA (1997) The Role of the Pyrazolate Ligand in Building Polynuclear Transition Metal Systems. In: Prog. Inorg. Chem. Vol. 46. pp 151–238
2. Meyer F (2006) Clues to Dimetallohydrolase Mechanisms from Studies on Pyrazolate-Based Bioinspired Dizinc Complexes – Experimental Evidence for a Functional Zn–O2H3–Zn Motif. Eur J Inorg Chem 2006:3789–3800. doi: 10.1002/ejic.200600590
3. Toubala K., Boukabcha N., Tamer Ö., Benhalima N., Altürk S., Avcı D., Chouaih A., Atalay Y., Djafri A., Hamzaoui F. (2017) Spectroscopic (FT-IR,1H and 13C NMR) characterization and density functional theory calculations for (Z)-5-(4-nitrobenzyliden)-3-N(2-ethoxyphenyl)-2-thioxo-thiazolidin-4-one (ARNO), J. Mol. Struct. 1147, 569-581.
4. Mohamed A a, Burini A, Fackler JP (2005) Mixed-metal triangular trinuclear complexes: dimers of gold-silver mixed-metal complexes from gold(I) carbeniates and silver(I) 3,5-diphenylpyrazolates. J Am Chem Soc 127:5012–3. doi: 10.1021/ja0429869
5. Omary M a, Rawashdeh-Omary M a, Gonser MWA, et al (2005) Metal effect on the supramolecular structure, photophysics, and acid-base character of trinuclear pyrazolato coinage metal complexes. Inorg Chem 44:8200–10. doi: 10.1021/ic0508730
6. Dias HVR, Diyabalanage HVK, Eldabaja MG, et al (2005) Brightly phosphorescent trinuclear copper(I) complexes of pyrazolates: substituent effects on the supramolecular structure and photophysics. J Am Chem Soc 127:7489–501. doi: 10.1021/ja0427146
7. Hu B, Gahungu G, Zhang J (2007) Optical properties of the phosphorescent trinuclear copper(I) complexes of pyrazolates: insights from theory. J Phys Chem A 111:4965–73. doi: 10.1021/jp0689215
8. Goikhman R, Jacques TL, Sames D (2009) C-H bonds as ubiquitous functionality: a general approach to complex arylated pyrazoles via sequential regioselective C-arylation and N-alkylation enabled by SEM-group transposition. J Am Chem Soc 131:3042–8. doi:

10.1021/ja8096114

9. Karrouchi K., Radi S., Ramli Y., Taoufik J., Mabkhot Y, Al-aizari F. and Ansar M. (2018) Synthesis and Pharmacological Activities of Pyrazole Derivatives: A Review, Molecules, 23, 134.

10. Bustos C, Schott E, Ríos M, et al (2009) Facile Synthesis Of Isoxazoles And Pyrazoles From B-Diketohydrazones. J Chil Chem Soc 54:267–268.

11. Miller RD, O. Reiser (1993) The synthesis of Electron Donor-Acceptor Substituted Pyrazoles. J Heterocycl Chem 30:755–763.

12. Makino K, Kim HS, Kurasawa Y (1998) Synthesis of Pyrazoles. J Heterocycl Chem 35:489–497.

13. Mukherjee R (2000) Coordination chemistry with pyrazole-based chelating ligands: molecular structural aspects. Coord Chem Rev 203:151–218. doi: 10.1016/S0010-8545(99)00144-7

14. Otero A, Fernández-Baeza J, Lara-Sánchez A, et al (2008) Recent Advances in the Design and Coordination Chemistry of Heteroscorpionate Ligands Bearing Stereogenic Centres. Eur J Inorg Chem 2008:5309–5326. doi: 10.1002/ejic.200800710

15. Klingele J, Dechert S, Meyer F (2009) Polynuclear transition metal complexes of metal···metal-bridging compartmental pyrazolate ligands. Coord Chem Rev 253:2698–2741. doi: 10.1016/j.ccr.2009.03.026

16. Elguero J, Alkorta I, Claramunt RM, et al (2009) Theoretical calculations of a model of NOS indazole inhibitors: interaction of aromatic compounds with Zn-porphyrins. Bioorg Med Chem 17:8027–31. doi: 10.1016/j.bmc.2009.10.006

17. Trofimenko S (2004) Scorpionates: genesis, milestones, prognosis. Polyhedron 23:197–203. doi: 10.1016/j.poly.2003.11.013

18. Kiviniemi S, Sillanp A, Nissinen M, et al (1999) Polar crystals with one-dimensional arrays from achiral components : crystal structures of 2:2 complexes of dibenzo-18-crown-6 –imidazolium and pyrazolium perchlorates. Chem Commun 897–898.

19. Kiviniemi S, Nissinen M, Lämsä MT, et al (2000) Complexation of planar, organic, five-membered cations with crown ethers. New J Chem 2000:47–52.

20. Kiviniemi S, Nissinen M, Alaviuhkola T, et al (2001) The complexation of tetraphenylborate with organic N-heteroaromatic cations. J Chem Soc Perkin Trans 2 6:2364–2369. doi: 10.1039/b100775k

21. Ardizzoia GA, LaMonica G, Maspero A, et al (1998) Pyrazolato Metal Complexes: Synthesis, Characterization and X-ray Crystal Structures of Rhenium(I) Derivatives. Eur J Inorg Chem 1998:1503–1512. doi: 10.1002/(SICI)1099-0682(199810)1998:10<1503::AID-EJIC1503>3.0.CO;2-0

22. Falvello LR, Fornie J, Martín A, et al (2002) Synthesis and Reactivity of the Neutral Pyrazolate Complexes [M2{CH2C6H4P(o-tolyl)2-KC,P}2(μ-Rpz)2] (M=Pd, Pt; Rpz=Pz, 3,5-dmpz, 4-Mepz) toward AgClO4. Molecular Structure of [Pt2Ag{CH2C6H4P(o-tolyl)2-KC,P}2(μ-4-Mepz)2]ClO4. Organometallics 21:4604–4610.

23. Budzisz E, Krajewska U, Rozalski M, et al (2004) Biological evaluation of novel Pt(II) and Pd(II) complexes with pyrazole-containing ligands. Eur J Pharmacol 502:59–65. doi: 10.1016/j.ejphar.2004.08.053

24. Gasser G, Ott I, Metzler-Nolte N (2011) Organometallic anticancer compounds. J Med Chem 54:3–25. doi: 10.1021/jm100020w

25. Keter FK, Darkwa J (2012) Perspective: The potential of pyrazole-based compounds in medicine. BioMetals 25:9–21. doi: 10.1007/s10534-011-9496-4

26. Budzisz E, Malecka M, Nawrot B (2004) Synthesis and structure of highly substituted pyrazole ligands and their complexes with platinum(II) and palladium(II) metal ions. Tetrahedron 60:1749–1759. doi: 10.1016/j.tet.2003.12.044

27. Yousef TA, Abu El-Reash GM, Al-Jahdali M, El-Rakhawy EBR (2014) Synthesis, spectral characterization and biological evaluation of Mn(II), Co(II), Ni(II), Cu(II), Zn(II) and Cd(II) complexes with thiosemicarbazone ending by pyrazole and pyridyl rings. Spectrochim Acta - Part A Mol Biomol Spectrosc 129:163–172. doi: 10.1016/j.saa.2014.02.184

28. Umakoshi K, Yamauchi Y, Nakamiya K, et al (2003) Pyrazolato-Bridged Polynuclear Palladium and Platinum Complexes. Synthesis , Structure , and Reactivity. Inorg Chem 42:3907–3916.

29. Ansari A., Ali A., Asif M. and Shamsuzzaman (2017) Review: biologically active pyrazole derivatives. New. J. Chem. 41, 16.

30. Yao HC (1964) Azohydrazone Conversion. II. The Coupling of Diazonium Ion with β-Diketones. J Am Chem Soc 29:2959–2963.

31. Bertolasi V, Gilli P, Ferretti V, Vaughan K (1999) Interplay between steric and electronic factors in determining the strength of intramolecular resonance-assisted NH...O hydrogen bond in a series of b-ketoarylhydrazones. New J Chem 23:1261–1267.

32. Farrugia LJ (1999) WinGX suite for small-molecule single-crystal crystallography. J Appl Crystallogr 32:837–838. doi: 10.1107/S0021889899006020

33. Burla MC, Caliandro R, Camalli M, et al (2005) SIR2004 : an improved tool for crystal structure determination and refinement. J Appl Crystallogr 38:381–388. doi: 10.1107/S002188980403225X

34. Sheldrick GM (1990) Phase annealing in SHELX-90: direct methods for larger structures. Acta Crystallogr Sect A Found Crystallogr 46:467–473. doi: 10.1107/S0108767390000277

35. M.J. Frisch, G.W. Trucks, H.B. Schlegel, P.M.W. Gill, B.G. Johnson MAR, J.R. Cheeseman,

T.A. Keith, G.A. Petersson, J.A. Montgomery, K. Raghavachari MA, Al-Laham, V.G. Zakrzewski, J.V. Ortiz, J.B. Foresman, J. Cioslowski BBS, et al Gaussian 03, Revision C.02, Gaussian, Inc., Wallingford, CT, EUA.

36. Becke AD (1996) Density-functional thermochemistry. IV. A new dynamic correlation functional and implications for exact-exchange mixing. J Chem Phys 104:1040–1046. doi: 10.1063/1.470829

37. Lee C, Yang W, Parr RG (1988) Development of the Colle-Salvetti correlation-energy formula into a functional of the electron density. Phys Rev B 37:785–789.

38. Miehlich B, Savin A, Stoll H, Preuss H (1989) Results obtained with the correlation energy density functionals of becke and Lee, Yang and Parr. Chem Phys Lett 157:200–206. doi: 10.1016/0009-2614(89)87234-3

39. Becke AD (1993) Density-functional thermochemistry. III. The role of exact exchange. J Chem Phys 98:5648–5652. doi: 10.1063/1.464913

40. Yanai T, Tew DP, Handy NC (2004) A new hybrid exchange-correlation functional using the Coulomb-attenuating method (CAM-B3LYP). Chem Phys Lett 393:51–57. doi: 10.1016/j.cplett.2004.06.011

41. Hay PJ, Wadt WR (1985) Ab initio effective core potentials for molecular calculations. Potentials for the transition metal atoms Sc to Hg. J Chem Phys 82:270. doi: 10.1063/1.448799

42. Cossi M, Scalmani G, Rega N, Barone V (2002) New developments in the polarizable continuum model for quantum mechanical and classical calculations on molecules in solution. J Chem Phys 117:43. doi: 10.1063/1.1480445

43. Faundez-Gutierrez R, Macleod-Carey D, Zarate X, et al (2014) Synthesis, characterization and DFT study of a new family of pyrazole derivatives. Polyhedron 81:414–420. doi: 10.1016/j.poly.2014.06.003

44. Sikorski A, Trzybiński D (2013) Networks of intermolecular interactions involving nitro groups in the crystals of three polymorphs of 9-aminoacridinium 2,4-dinitrobenzoate • 2,4-dinitrobenzoic acid. J Mol Struct 1049:90–98. doi: 10.1016/j.molstruc.2013.06.031

45. K. Pluta, M. Jeleń, B. Morak-Młodawska, M. Zimecki, J. Artym, M. Kocięba Anticancer activity of newly synthesized azaphenothiazines in NCI's anticancer screening Pharmacol. Rep., 62 (2010), pp. 319-332

46. Pearson RG (1992) The electronic chemical potential and chemical hardness. J Mol Struct THEOCHEM 255:261–270. doi: 10.1016/0166-1280(92)85014-C

47. Parr RG, Szentpaly L, Liu S (1999) Electrophilicity index. J Am Chem Soc 121:1922–1924. doi: 10.1021/cr040109f

48. Chattaraj PK, Giri S (2009) Electrophilicity index within a conceptual DFT framework. Annu

Rep Prog Chem{,} Sect C Phys Chem 105:13–39. doi: 10.1039/B802832J

49. Hansch C, Leo A, Taft RW (1991) A survey of Hammett substituent constants and resonance and field parameters A Survey of Hammett Substituent Constants and Resonance and Field Parameters. Chem Rev 91:165–195. doi: 10.1021/cr00002a004

- Twelve (E)-3,5-dimethyl-1-(4-**R**-phenyl)-4-(phenyldiazenyl)-1H-pyrazoles were synthesized and characterized by the spectroscopy of ^{1}H NMR, ^{13}C NMR, IR, UVVIS and EA.
- The crystal structure of three of them was determined.
- The synthesized compounds were evaluated their anticancer abilities against 60 cell lines.
- DFT and TDDFT calculation were performed.

Synthesis, characterization and biological trials of pyrazoles with general name (E)-3,5-dimethyl-1-(4-R-phenyl)-4-(phenyldiazenyl)-1H-pyrazoles (with R= 4-CH_3O (**1**), 4-CH_3 (**2**), 4-H (**3**), 4-F (**4**), 4-Cl (**5**), 4-CF_3 (**6**), 4-CN (**7**), 4-NO_2 (**8**), 3-Cl (**9**), 3-NO_2 (**10**), 2-Cl (**11**) and -C_6F_5 (**12**)). The structures of **4**, **5** and **8** were reached by X-Ray diffraction. Also, molecular/electronic structure was tuned by means of changing the -R substituent. Biological activity, specifically anticancer were observed against cancer cell lines (60), including leukemia, colon and brain cancer.